An alternative route towards micro- and nano-patterning of oxide films

2012 Nanotechnology 23 085302

(http://iopscience.iop.org/0957-4484/23/8/085302)

Nanotechnology **23** (2012) 085302 (7pp) doi:10.1088/0957-4484/23/8/085302

An alternative route towards micro- and nano-patterning of oxide films

G Bridoux[1], J Barzola-Quiquia[1], F Bern[1], W Böhlmann[1], I Vrejoiu[2], M Ziese[1] and P Esquinazi[1]

[1] Division of Superconductivity and Magnetism, University of Leipzig, Linnéstrasse 5, D-04103 Leipzig, Germany
[2] Max-Planck-Institut für Mikrostrukturphysik, D-06120 Halle, Germany

E-mail: gbridoux@yahoo.com.ar and esquin@physik.uni-leipzig.de

Received 9 September 2011, in final form 12 January 2012
Published 1 February 2012
Online at stacks.iop.org/Nano/23/085302

Abstract
This paper presents a method to obtain submicron- and nanometer structures of different oxide films and heterostructures combining e-beam lithography and chemical etching. The most relevant advantage of this method is that structures of tens of microns in length and below ∼100 nm width can be produced, keeping the intrinsic bulk film properties, as proven by electrical transport measurements. In this way our method provides a bridge that connects the attractive properties of oxide films and the nanoworld.

(Some figures may appear in colour only in the online journal)

1. Introduction

The development of oxide materials has been one of the important engines in solid state physics during the last decades. From semiconducting [1], superconducting [2] to ferromagnetic and ferroelectric oxides [3], all the main condensed matter fields were boosted by these compounds. On the other hand, a broad application of oxide thin films and multilayers within nanotechnology still remains a challenge. Thin films play a key role in the development of these devices. Therefore, it is extremely important to have a simple, inexpensive and reliable method to build micron-, submicron- and nanostructures of different oxide films. The aim of this work is to present a method that combines lithography and chemical etching to obtain submicron- and nanopatterns in different oxide films and heterostructures. In particular we have used electron-beam (e-beam) lithography due to the flexibility in the final patterns that can be drawn in the electron-beam resist: however, similar results can be achieved using other lithography techniques.

Many efforts for micro- and nano-patterning of oxide films have been made in recent years. One possibility is the use of *in situ* nano-patterning during the oxide film growth but this possibility has not materialized yet. A combination of e-beam lithography and ion-beam etching is the option that many groups have chosen nowadays [4–6]. However, the drawback of this method is the ion contamination that the thin film suffers during patterning, losing in this way its intrinsic properties. We describe here an experimental method that combines e-beam lithography with wet chemical etching, allowing us to create micron-, submicron- and nanostructures in different oxide films such as $La_{1-x}Ca_xMnO_3$ (LCMO), $La_{1-x}Sr_xMnO_3$ (LSMO), $YBa_2Cu_3O_{7-\delta}$ (YBCO), ZnO, Fe_3O_4 and $PbZr_{1-x}Ti_xO_3$ (PZT) avoiding any contamination. Other groups have tried a similar approach in some of the above-mentioned compounds [7–10]. However, in contrast to those works, our method allows us to study oxide materials at micron-, submicron- and nanometer length scales with well-defined cross sections and small roughness, as demonstrated in the following sections. As an example, in section 4 of this paper the evolution of the electric transport properties of ferromagnetic metallic $La_{0.7}Sr_{0.3}MnO_3$ is described as a function of wire width from ∼100 μm down to ∼0.1 μm.

2. Experimental details

The first step is to check if the e-beam resist (PMMA 950K, AR-P 671-05) layer remains intact after the immersion in the corresponding acid solution that will constitute the etchant for the particular oxide material. This procedure has been checked successfully for all the acid solutions investigated, see table 1.

After this, an e-beam writes an arbitrary pattern on the resist that covers the oxide film. The parts of the PMMA

Table 1. Some of the oxide film materials used in this work to produce micro- and nanostructures and the corresponding acid solutions and etching rates. The expected chemical reactions are listed in the appendix.

Oxide film	Oxide bilayer or multilayer	Acid solution	Etching rate (nm s^{-1})
$La_{0.7}Ca_{0.3}MnO_3$		4 ml HCl 35 wt% +4 ml KI 3 M in H_2O + 70 ml H_2O	∼35
$La_{0.7}Sr_{0.3}MnO_3$			
ZnO		50 ml H_3PO_4 85 wt% in H_2O + 50 ml H_2O	∼60
$Zn_{1-x}Co_xO$			
$Zn_{1-x}Mn_xO$			
$Zn_{1-x}Mg_xO$			
$YBa_2Cu_3O_7$		1 g (2.53 mmol) $C_{10}H_{14}N_2Na_3O_{8.2}H_2O$ + 70 ml H_2O at 80 °C	∼50
$GdBa_2Cu_3O_7$			
$PrBa_2Cu_3O_7$			
Fe_3O_4		5 ml HCl 35 wt% in H_2O + 20 ml HF 48 wt% in H_2O + 70 ml H_2O at 70 °C	∼200
Fe_2O_3			
$ZnFe_2O_4$			
	$La_{0.7}Sr_{0.3}MnO_3/PbZr_{0.2}Ti_{0.8}O_3$	60 ml HCl 35 wt% in H_2O + 4 ml KI 3 M in H_2O + 900 ml H_2O + 6 ml 7:1 NH_4F:HF (0.85 ml 48% HF, 0.19 g of NH_4F in 5.15 ml of H_2O = 5.15 mmol) + 60 ml acetic acid + 60 ml HNO_3 + 16 g (0.04 mol) EDTA trisodium + 40 g (0.75 mol) NH_4Cl	∼1

exposed to the e-beam are removed using the corresponding developer (AR 600-55). The regions of the film covered by this resist will be protected from the acid solution, while the rest of the film will be removed after immersion in the corresponding acid solution, as can be seen in the images of figures 1(a) and (b). Following this procedure and tuning the solution concentration and the etching rate for each oxide film (see table 1), a controlled design of micro- and nano-patterns can be achieved, see the images in figures 1(c)–(e). Table 1 summarizes the most concentrated solutions we have used (with the higher etching rates). However, we have checked that the dilution of these ones leads to lower etching rates without degradation of the nanostructural features. A linear relation between the total thickness of the oxide film (ranging from 20 to 500 nm) and the total immersion time in its corresponding acid solution has also been proved. It is also important to note that, in all the fabricated submicron structures, the total etching time for a particular etching solution is always much less than the time required to produce an etching of the oxide substrate. This was verified by immersing different substrates ($SrTiO_3$, Al_2O_3, etc) with a patterned PMMA on top in the etching solutions listed in table 1 during several minutes, resulting in unchanged surfaces.

3. Results and discussion

3.1. General characteristics of the patterned structures

The AFM and SEM images of figures 2 and 3 show some of the main features of the structures. In figure 2, AFM images show an LSMO structure varying in width continuously from several tens of microns down to ∼470 nm. Figures 3(a) and (c) present AFM images of LSMO nanoconstrictions of ∼64 nm and ∼300 nm width, respectively. Relevant characteristics of the fabricated structures are the sharpness of the edges, the well-defined cross section, see figures 2 and 3(e), the small roughness and the large extension along one direction, as can be noticed in figure 2.

The cross-section profiles of figures 2 and 3(e) show a sloping angle $\alpha \sim 35\,^{\circ}$C, a feature that is present in all the fabricated nanostructures. Hence, for a fixed patterned width on the PMMA (minimum width $\leq$ 100 nm), w_{PMMA}, the resulting width of the oxide film, w, is approximately equal to the difference between w_{PMMA} and $2t\tan(\alpha)$, where t is the total thickness of the oxide film. We have experimentally verified this relation for all the oxide films listed in table 1 (with thicknesses from 20 to 500 nm) with their corresponding chemical etchant (also listed in table 1). On the other hand, if the etching process is isotropic $\alpha \sim 45\,^{\circ}$C. However, in our nanostructures it seems that the etching rate in the vertical direction (listed in table 1) is $\sim\cot 35^{\circ} = 1.43$ times larger than in the horizontal direction. Our starting oxide thin films were mainly grown by pulsed laser deposition (PLD) and post-annealed in oxygen atmosphere above 300 °C in most of the cases, resulting in epitaxial or textured films with a high crystalline anisotropy [11–15] that is reflected in their physical and chemical properties. Hence we do not discard the possibility that the chemical solutions listed in table 1 etch in a preferential crystalline direction of our oxide thin films. A detailed explanation of this mechanism is beyond the scope of this work.

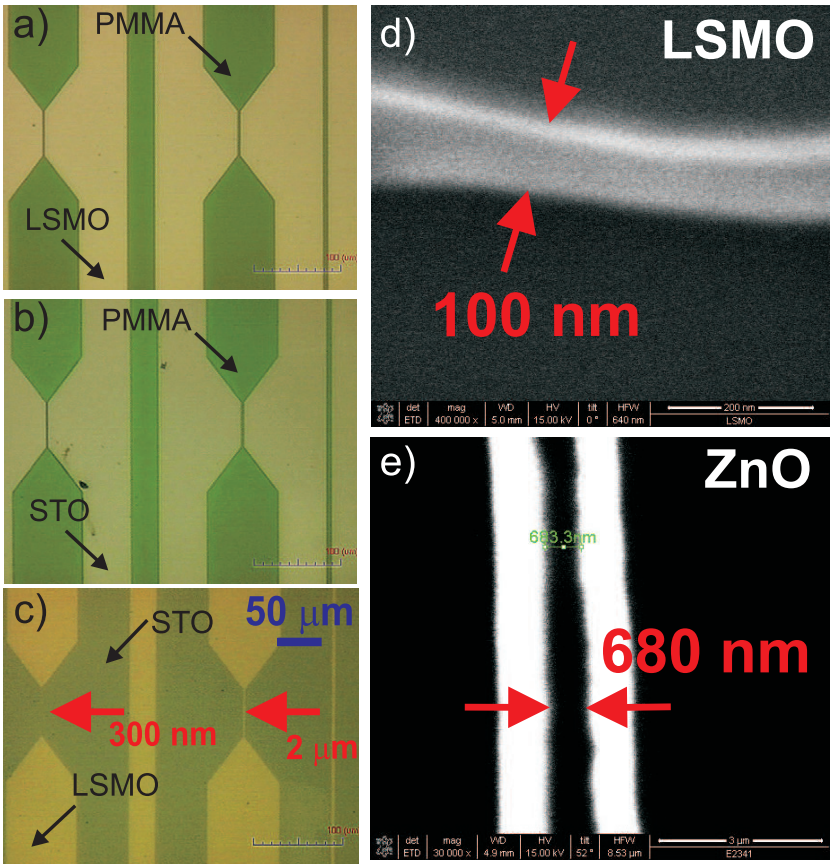

Figure 1. (a)–(d) Micro- and nano-patterning of an $La_{0.7}Sr_{0.3}MnO_3$ thin film grown on an $SrTiO_3$ substrate. (a) Before etching: the green regions correspond to the PMMA that protects the LSMO thin film. (b) After etching: the LSMO thin film was removed from the regions uncovered by the PMMA. As can be seen, the PMMA remained unaffected by the acid attack. (c) Micro- and nano-patterns obtained in LSMO after the PMMA removal. (d) SEM image of a ∼100 nm wide LSMO nanowire with a thickness of 35 nm. (e) For comparison: SEM image of a ∼680 nm wide ZnO nanowire with a thickness of about 60 nm.

The patterning method presented in this work is not limited to the development of nanostructures in one-compound films. The design and fabrication of nanostructures in oxide superlattices is also possible. Figure 3(b) shows a ∼800 nm wide and ∼50 nm thick wire produced by the present method, starting from a PZT/LSMO multiferroic heterostructure [11, 12]. With the patterning method it was possible to solve the problem of 'short-circuited layers' at the edges of the substrate [11, 12] providing new possibilities to study the perpendicular-to-plane electric transport properties of oxide heterostructures.

3.2. Size effects in a ferromagnetic LSMO film

In this section the magnetotransport properties of a patterned LSMO film are discussed. Since the transport properties of manganites sensitively depend on the electron-defect interaction and electron–phonon coupling, transport measurements are a versatile tool to assess structural deficiencies introduced by the patterning procedure. Here temperature-dependent resistivity measurements are used to assess changes in the intrinsic transport measurements, whereas magnetoresistance measurements are used to probe size effects on the magnetic domain patterns. The latter are expected, since the final lateral size of 470 nm is of the order of the typical size of magnetic domains.

Figure 4 shows the normalized resistivity as a function of temperature for the 35 nm thick, ∼470 nm wide LSMO wire, characterized before by the AFM images in figures 2(a)–(c) in comparison with the full film before patterning. Both curves exhibit the typical metallic-like behavior below the ferromagnetic transition ($T_c \simeq 360$ K) [16] and agree in the whole range of temperature. This is an outstanding finding, which implies that the intrinsic film properties remain unaffected when going from the as-prepared film to the submicrometer structure. Within experimental resolution one might conclude that our fabrication method avoids any contamination or degradation of the original film. These data confirm that the scattering mechanisms for the carriers, dominated by magnon scattering processes [3], do not change when the width of the LSMO strip is reduced to the order of ∼500 nm.

In order to check for the existence of size effects we have studied the magnetoresistance $MR = (R(H) - R(0))/R(0)$ in LSMO bridges of different widths, namely 80, 2 μm and 470 nm. In figure 5 the magnetic field dependence of the MR for the three samples is presented. Figure 5(a) shows

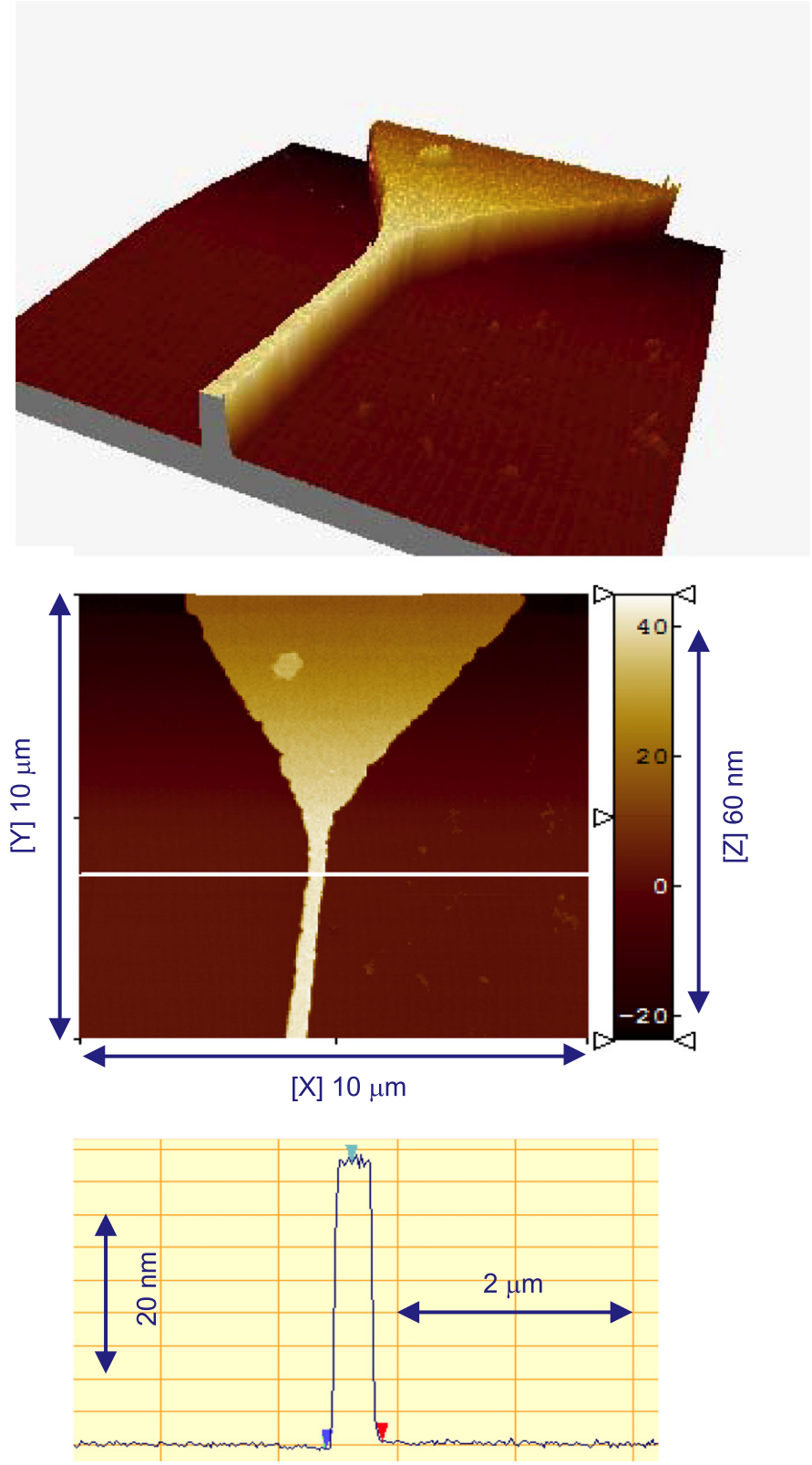

Figure 2. AFM images of a continuous LSMO structure varying in width from several tens of microns down to ∼470 nm. The bottom trace shows a cross section of the nanostructure (thickness ∼ 35 nm). From this trace one can estimate that the sloping angle is at least 35 °C, a lower limit set by the rounding of the AFM tip.

the corresponding data for magnetic fields H perpendicular to the film plane and perpendicular to the electrical current density J, whereas figure 5(b) shows the in-plane MR data for the magnetic field parallel to the current density. In both field orientations the high field magnetoresistance is negative and does not depend on the width of the LSMO bridge, in agreement with the results of figure 4, showing again that the intrinsic transport properties are not affected by the patterning.

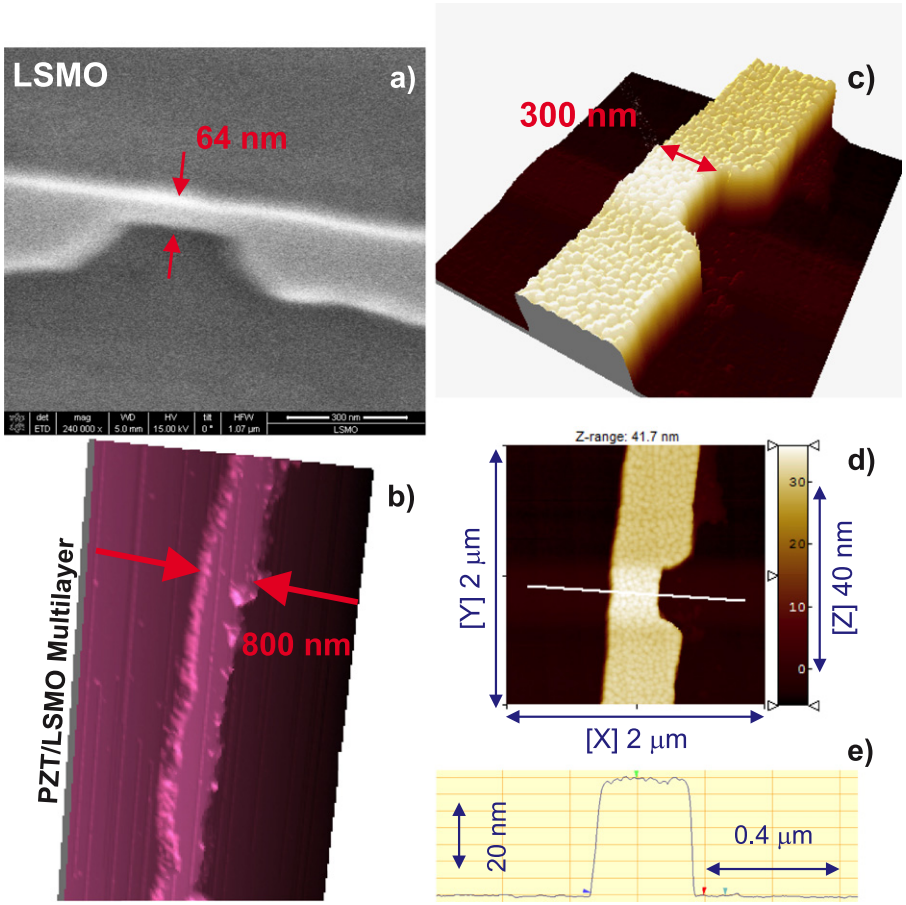

Figure 3. Nanoconstrictions and oxide superlattice nanowires. (a) SEM image of a ∼64 nm wide LSMO nanoconstriction. (b) SEM image of a ∼800 nm wide PZT/LSMO superlattice nanowire (thickness ∼ 50 nm). (c) and (d) AFM images of a ∼300 nm wide LSMO constriction. Its corresponding cross section is shown in (e) (thickness ∼ 35 nm).

The low field magnetoresistance depends on the sample width as can be seen in the low field region of figure 5 and in more detail in figure 6. Figure 6(a) shows the transverse magnetoresistance for magnetic fields perpendicular to the film plane. The MR at low fields is positive and reaches a maximum at H_{max} as reported before for unpatterned LCMO films [17]. Phenomenologically, the observed behavior was addressed as arising from anisotropic magnetoresistance and can be explain as follows [17, 18]. LSMO and LCMO films—grown under tensile strain on $SrTiO_3$ substrates—have only a weak magnetocrystalline anisotropy such that the dominating shape anisotropy keeps the magnetization parallel to the film. In order to estimate the resistance change with magnetic field we need to take into account that a magnetic field H applied normal to the film plane rotates the magnetization vector of each of the magnetic domains towards the surface normal by an angle Θ (measured with respect to the surface normal) given by $\cos\Theta \propto H/(1 + (H_K/M_S))$, where $H_K = 2K_\perp/(\mu_0 M_S)$ is the effective anisotropy field, $K_\perp$ is the magnetocrystalline anisotropy constant and M_S is the saturation magnetization. Therefore, the magnetization rotation from the in-plane to the perpendicular-to-plane direction leads to a resistivity increase at low fields $\Delta\rho \propto \cos^2\Theta \propto H^2$, which is indeed observed in the 470 nm wide sample, see figure 6(a).

Details of the field dependence and magnitude of the resistivity increase depends on the micromagnetic structure, the degree of tetragonal distortion of the film, the value of the magnetocrystalline anisotropy and the alignment of the applied field with the surface normal. The anisotropic magnetoresistance (AMR) is, in general, larger for magnetization rotations from the in-plane longitudinal ($\vec{H} \parallel \hat{I}, \hat{I}$ is the in-plane current direction) to the perpendicular transverse direction than for rotations from the in-plane transverse ($\vec{H} \perp \hat{I}$) to the perpendicular transverse direction. Therefore the difference in the positive MR values between the 80 μm wide and the narrower samples indicates a preferential orientation of the magnetization along the sample axis in the case of the 2 μm and 470 nm wide samples. Whereas in the 80 μm wide sample the orientation of the in-plane magnetic domains are at random. This is in agreement with observations of the typical magnetic domains size in LSMO of about 1 μm [19–21]. The deviations from the quadratic field dependence at low fields is very probably due to the influence of a parallel field component due to the misalignment of the applied field.

The field H_{max}, corresponding to the MR maximum in the perpendicular-to-plane configuration, is determined by the competition between the positive anisotropic MR explained above and the negative colossal MR (CMR). Since the CMR

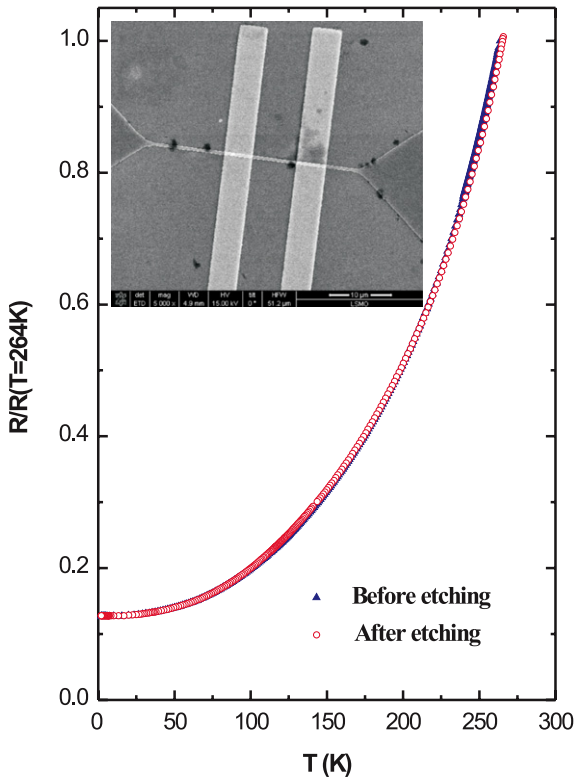

Figure 4. Temperature dependence of the electrical resistivity of the LSMO nanowire shown in figures 2(a)–(c) and of the corresponding full film normalized to the respective values at 264 K. The symbols correspond to: (full triangle): pristine LSMO film, before etching and ◯: LSMO wire, after etching. The inset shows a SEM image of the voltage contacts consisting of Au electrodes deposited onto the nanowire.

depends on the magnetization changes induced by the applied magnetic field, H_{max} is strongly influenced by the anisotropy constant $K_{\perp}$ as well as by the micromagnetic structure. These factors lead to deviations of the internal magnetic field $B/\mu_0 = H - M$ from the value one would have obtained in a homogeneously magnetized films in a perpendicular field. Therefore changes in H_{max} are not straightforward to interpret and do not correspond to the coercive fields.

Figure 6(b) shows the MR of the stripes for field parallel to the film. The peak in the MR occurs at the coercive field H_c, in contrast to the perpendicular direction. The data show a shift of H_c to higher fields when the width of the stripes is reduced, in agreement with a shape anisotropy contribution, previously seen in Co and NiFe nanowires [22, 23]. Note, however, that our H_c values are in disagreement with those calculated for LSMO nanowires assuming only a shape anisotropy contribution [24], indicating that domain-wall pinning [25] and/or buckling of the magnetic moments [26] should be taken into account to understand the increase of the coercive field with decreasing wire width.

4. Conclusion

This paper provides a new path for the nano-patterning of oxide materials. The combination of e-beam lithography and wet-etching techniques allows for the design and fabrication of oxide micro- and nanostructures, starting from a thin film or multilayer and avoiding any contamination. In particular, electrical transport measurements of LSMO submicrometer structures reveal that the micromagnetic structure affects the magnetoresistance at sample sizes below 2 μm.

Acknowledgments

We thank H Hochmuth and M Lorenz for providing some of the oxide thin films. This work was supported by the DFG through the Sonderforschungsbereich SFB 762. Patent pending: German Patent Office application no. 10 2009 045 114.5 (2009).

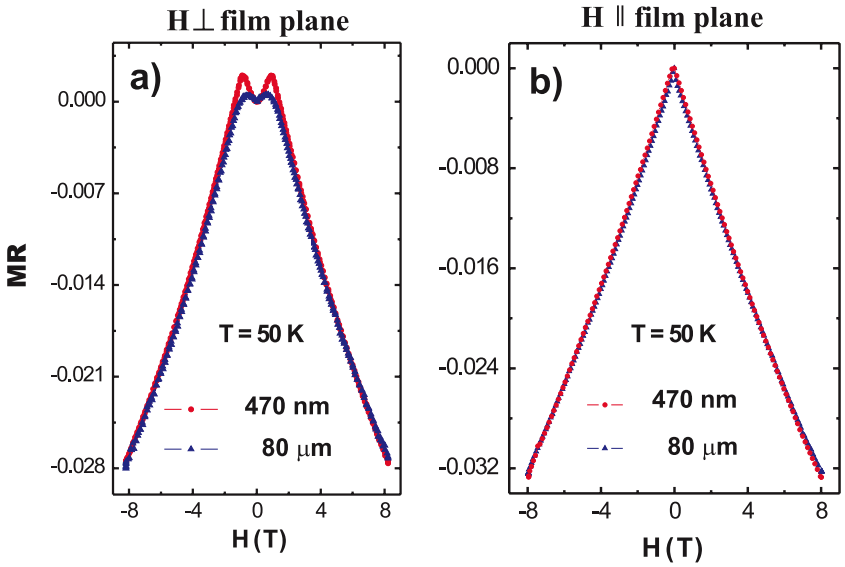

Figure 5. High field magnetoresistance, MR $= (R(H) - R(H = 0))/R(H = 0)$ in $La_{0.7}Sr_{0.3}MnO_3$ bridges 470 nm (red circles) and 80 μm (blue triangles) wide at $T = 50$ K for (a) $H \perp$ film plane, $H \perp J$ and (b) $H \parallel$ film plane, $H \parallel J$.

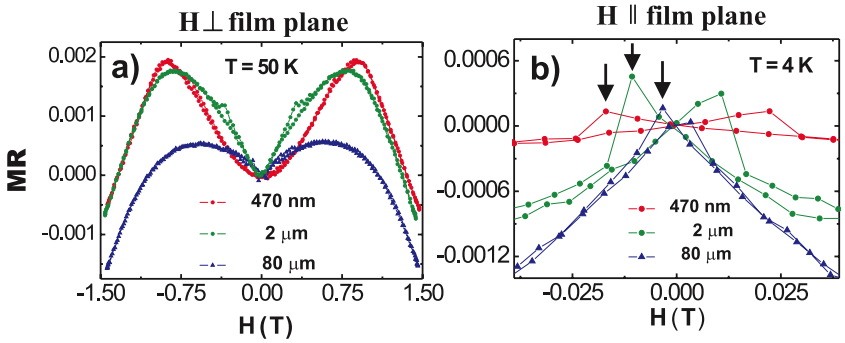

Figure 6. Low magnetic field magnetoresistance, MR $= (R(H) - R(H = 0))/R(H = 0)$ in $La_{0.7}Sr_{0.3}MnO_3$ stripes 470 nm (red circles), 2 μm (green circles) and 80 μm (blue triangles) wide for (a) $H \perp$ film plane, $H \perp J$ at $T = 50$ K and (b) $H \parallel$ film plane, $H \parallel J$ at $T = 4$ K.

Appendix

The possible chemical reactions that have taken place are:

$La_{0.7}Ca_{0.3}MnO_3 + H_2O + 5HCl + KI \rightarrow MnCl_2 + Cl_2 + 1/2I_2 + KOH + 3H_2O + La_{0.7}Ca_{0.3}Cl$

$ZnO + 2H_2O + H_3PO_4 \rightarrow ZnHPO_4 + 3H_2O$

$YBa_2Cu_3O_7 + H_2O + 2Na_3(EDTA) \rightarrow [YBa_2Cu_3]_3(EDTA) + 6NaOH + H_2O.$

Note that $C_{10}H_{13}N_2Na_3O_8$ is equivalent to $Na_3(EDTA)$.

$2Fe_3O_4 + 8HCl + 8HF + H_2O \rightarrow 2FeCl_3 + FeCl_2 + 2FeF_3 + FeF_2 + 9H_2O$

$PbZr_{0.2}Ti_{0.8}O_3 + Na_3(EDTA) + NH_4Cl + H_2O +$ aceticacid$+ HNO_3 + HCl +$ 7:1 NH_4F:HF$\rightarrow [PbZr_{0.2}Ti_{0.8}]_3(EDTA) + NH_4OH + NaOH \cdots +$ a mixture of different salts like titanium acetate, titanium nitrate, titanium chloride/-fluoride, lead acetate, lead chloride/fluoride, -nitrate and water. We remark that the whole mixture is a buffer solution to guarantee that the pH value is nearly constant. Therefore, the mixture is made of different acids and salts.

References

[1] Grundmann M 2006 *The Physics of Semiconductors* (Heidelberg: Springer)

[2] Bednorz J G and Müller K A 1986 *Z. Phys.* B **64** 189

[3] Salamon M B and Jaime M 2001 *Rev. Mod. Phys.* **73** 583

[4] Ono T, Kogusu A, Morimoto S, Nasu S, Masuno A, Terashima T and Takano M 2004 *Appl. Phys. Lett.* **84** 2370

[5] Arnal T, Khvalkovskii A V, Bibes M, Mercey B, Lecoeur Ph and Haghiri Gosnet A-M 2007 *Phys. Rev.* B **75** 220409

[6] Walsh M E, Hao Y, Ross C A and Smith H I 2000 *J. Vac. Sci. Technol.* B **18** 3539

[7] Ballentine P H, Kadin A M, Fisher M A, Mallory D S and Donaldson W R 1989 *IEEE Trans. Magn.* **25** 950

[8] Liu W, Ko J and Zhu W 2000 *J. Mater. Sci. Lett.* **19** 2263

[9] Shokoohi F K, Schiavone L M, Rogers C T, Inam A, Wu X D, Nazar L and Venkatesan T 1989 *Appl. Phys. Lett.* **55** 2661

[10] Sun J R, Yeung C F, Zhao K, Wong H K, Xiong C M and Shen B G 2003 *Physica* B **334** 310 and references there in

[11] Vrejoiu I, Ziese M, Setzer A, Esquinazi P, Birajdar B I, Lotnyk A, Alexe M and Hesse D 2008 *Appl. Phys. Lett.* **92** 152506

[12] Ziese M, Setzer A, Vrejoiu I, Birajdar B I, Rodriguez B J and Hesse D 2008 *J. Appl. Phys.* **104** 063908

[13] Kaidashev E M, Lorenz M, von Wenckstern H, Rahm A, Semmelhack H C, Han K H, Benndorf G, Bundesmann C, Hochmuth H and Grundmann M 2003 *Appl. Phys. Lett.* **82** 3901

[14] Ziese M, Köhler U, Bollero A, Höhne R and Esquinazi P 2005 *Phys. Rev.* B **71** 18046(R)

[15] Eom C B, Marshall A F, Triscone J M, Wilkens B, Laderman S S and Geballe T H 1991 *Science* **251** 780 and references there in

[16] Kaplan T A and Mahanti S D 1999 *Physics of Manganites* (Berlin: Springer)

[17] Eckstein J N, Bozovic I, O'Donnell J, Onellion M and Rzchowski M S 1996 *Appl. Phys. Lett.* **69** 1312

[18] Dahlberg E D, Riggs K and Prinz G A 1988 *J. Appl. Phys.* **63** 4270

[19] Ziese M 2006 *Phys. Status Solidi* b **243** 1383

[20] Dho J and Hur N H 2007 *J. Magn. Magn. Mater.* **318** 23

[21] Mechin L, Simon Ch and Chakalov R A 2008 *Int. J. Nanotechnol.* **6** 818

[22] Kirk K J, Chapman J N, McVitie S, Aitchison P R and Wilkinson C D W 1999 *Appl. Phys. Lett.* **75** 3683

[23] Brands M and Dumpich G 2005 *J. Phys. D: Appl. Phys.* **38** 822

[24] Dolz M I, Bast W, Antonio D, Pastoriza H, Curiale J, Sanchez R D and Leyva A G 2008 *J. Appl. Phys.* **103** 083909

[25] Chikamuzi S 1978 *Physics of Magnetism* (Malabar, FL: Krieger)

[26] Martin J I, Nogues J, Liu K, Vicent J L and Schuller I K 2003 *J. Magn. Magn. Mater.* **256** 449